JCTC Journal of Chemical Theory and Computation

Article

pubs.acs.org/JCTC

Solvent Effects on Excited-State Structures: A Quantum Monte Carlo and Density Functional Study

Riccardo Guareschi,[†] Franca Maria Floris,*[,‡] Claudio Amovilli,*[,‡] and Claudia Filippi*[,†]

[†]MESA+ Institute for Nanotechnology, University of Twente, P.O. Box 217, 7500 AE Enschede, The Netherlands

[‡]Dipartimento di Chimica e Chimica Industriale, Università di Pisa, Via Giuseppe Moruzzi 3, 56124 Pisa, Italy

Supporting Information

ABSTRACT: We present the first application of quantum Monte Carlo (QMC) in its variational flavor combined with the polarizable continuum model (PCM) to perform excited-state geometry optimization in solution. Our implementation of the PCM model is based on a reaction field that includes both volume and surface polarization charges and is determined self-consistently with the molecular wave function during the QMC optimization of the solute geometry. For acrolein, acetone, methylenecyclopropene, and the propenoic acid anion, we compute the optimal exited-state geometries in water and compare our results with the structures obtained with second-order perturbation theory (CASPT2) and other correlated methods, and with time-dependent density functional theory (TDDFT). We find that QMC predicts a structural response to solvation in good agreement with CASPT2 with the only exception of the $\pi \rightarrow \pi^*$ state of acrolein where the robustness of the QMC geometry must be contrasted to the sensitivity of the perturbation result to the details of the calculation. As regards TDDFT, we show that all investigated functionals systematically overestimate the geometrical changes from the gas phase to solution, sometimes giving bond variations opposite in trend to QMC.

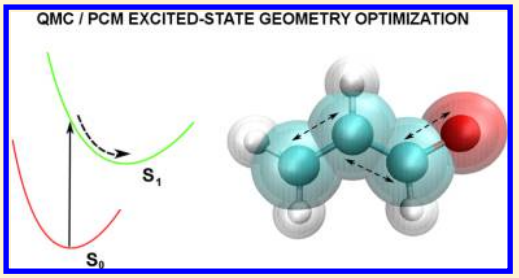

1. INTRODUCTION

A realistic theoretical description of photoexcitations in chemical systems must take into account that these processes generally occur in a condensed medium such as a liquid solution, which may significantly affect the molecular properties of the active species with respect to the gas phase. The most common approach to include solvation effects is to describe the solute at the quantum mechanical level and the solvent classically. In this framework, the solvent can be represented at different levels of sophistication, preserving its explicit atomistic structure or, at the other extreme, as a continuum medium.[1−7]

The methods based on a continuum solvent offer a cost-effective manner to approximately include an average description of the environment and account for important polarization contributions in processes such as absorption, emission, and structural relaxation in solution. Among the numerous variants of continuum approaches, the most popular nowadays is the polarizable continuum model (PCM),[1,6] where the solvent is a dielectric medium surrounding a molecule enclosed in a cavity and the solute−solvent interactions are mimicked via polarization charges distributed on the surface of the cavity and sometimes also in the bulk of the continuum medium (volume polarization charges).[1,8]

As regards the treatment of the solute and its structural response in the excited state, a plethora of quantum chemical methods is available whose performance has been primarily investigated in the gas phase. The ability of an approach to treat an isolated species does, however, not ensure an equally good quality of its excited-state response to the presence of a solvent. In benchmarking time-dependent density functional theory (TDDFT),[9−11] the focus has in fact recently moved to establish its performance in describing optimal excited-state structures, fluorescence emission, and adiabatic absorption beyond the gas phase. For this purpose, the combination of TDDFT with PCM techniques appears to be the simplest and most effective mean to obtain a fast, qualitatively correct analysis of molecular properties in a solvated environment and has, in fact, been employed to this purpose in different flavors,[12−19] the most recent one in a structural investigation also including the response of the exact TDDFT excited-state density.[20] These studies suffered, however, for the lack of good reference data, which can, in principle, be provided by accurate wave function methods.

In this context, quantum Monte Carlo (QMC) represents an accurate and robust highly correlated approach to investigate the properties of a solvated molecular system. QMC has been shown[21−26] to yield excitation energies of a variety of chromophores in good agreement with multireference second-order perturbation theories like CASPT2 in its most recent formulation[27] and the *n*-electron valence perturbation theory (NEVPT2),[28] while offering a more favorable scaling for large systems (N^4 with N the number of electrons) than either perturbation approach. Ground- and excited-state geometry optimizations[22,29−32] can be carried out within QMC in its variational (VMC) flavor thanks to a robust wave function

Received: August 8, 2014
Published: October 22, 2014

   dx.doi.org/10.1021/ct500723s | J. Chem. Theory Comput. 2014, 10, 5528−5537

optimization procedure in state-specific[33] and state-average[21] fashion, and an efficient implementation of the computation of interatomic forces with a finite-variance estimator.[29,30] Recently, our group has presented a detailed study of the ground- and excited-state geometry optimization of a set of representative organic molecules in the gas phase,[34] obtaining QMC optimal structures consistent with those resulting from perturbation theory and providing robust reference data whenever the application of a perturbation approach proved problematic.

The aim of this work is to provide an accurate PCM benchmark of both ground- and excited-state structures of prototypical organic solutes, which we treat here at the QMC level. For this purpose, we combine for the first time structural optimization in VMC with our QMC/PCM approach[35−38] to include a continuum solvent determined self-consistently with the solute wave function in terms of surface and volume polarization charges. For a set of small organic chromophores representative of $n \rightarrow \pi^*$ and $\pi \rightarrow \pi^*$ transitions, we compute the optimal excited-state geometries in water within VMC and compare them with those resulting from TDDFT and CASPT2 in the same medium. We find that QMC yields structural changes due to the presence of the solvent in good agreement with the predictions of the CASPT2 method. Furthermore, it provides a robust estimate of the geometry of the $\pi \rightarrow \pi^*$ state of acrolein, where the perturbation results are instead strongly dependent on the computational ingredients entering the calculation. Finally, all TDDFT functionals investigated here tend to overestimate the geometrical response to the solvent in the excited states and yield an even larger error with respect to the correlated approaches than in the gas phase.

The paper is organized as follows. In Section 2, we discuss various methodological aspects related to the computation of interatomic gradients in QMC/PCM, and in Section 3, we present the computational details. In Section 4, we present a detailed analysis of our results and conclude in Section 5.

2. METHODS

We focus here on the excited-state geometry optimization of small organic molecules and include solvation effects within the polarizable continuum model (PCM).[1,6,8,12,39−42] In this model, the molecule under study (the solute) is treated at the quantum mechanical level and placed inside a cavity made of a set of interlocking spheres generally centered on the atoms, which represents a boundary between the solute and the solvent. The solvent is represented as a continuum medium characterized by a static dielectric constant, ε, while the dielectric constant inside the cavity is equal to one. We assume a fast response of the solvent, namely, that the solvent molecules have time to undergo the orientational reorganization induced by the structural changes of the solute in the excited state.[1,38,39,42−44] Consequently, for water, we employ the static dielectric constant, $\varepsilon = 78.39$, in all excited-state geometrical optimizations.

2.1. QMC/PCM Approach. We investigate the effect of PCM solvation on the excited-state geometry within variational Monte Carlo (VMC), using our approach to accurately solve the Poisson equation coupled to a QMC description of the solute.[36,37]

Within the PCM, the electric field and the charge density of the solute is coupled to the electric field and the charge density of the solvent via the Poisson equation:

$$\nabla \cdot \mathbf{E} = 4\pi \rho^{\mathrm{tot}}(\mathbf{r}) \tag{1}$$

where $\mathbf{E}$ is the total electric field and $\rho^{\mathrm{tot}}(\mathbf{r})$ is the total charge density of the electrons and nuclei of the solute and the polarization density of the solvent. In our VMC/PCM calculations, we include surface polarization charges on the cavity as well as volume charges in the solvent region to accurately treat solvent polarization effects arising from the quantum mechanical spill-out of the solute electronic density from the cavity.

The volume polarization charge density outside the cavity is given by

$$\rho_{\mathrm{vol}}^{(\mathrm{pol})}(\mathbf{r}) = \left(\frac{1}{\varepsilon} - 1\right)\rho_{\mathrm{e}}(\mathbf{r}) \tag{2}$$

where $\rho_{\mathrm{e}}(\mathbf{r})$ is the electronic charge density of the solute. The electrostatic potential associated with this charge density is given by the following integral over the domain outside the cavity C

$$\begin{aligned}\phi_{\mathrm{vol}}^{\mathrm{pol}}(\mathbf{r}) &= \int_{\mathbf{r}' \notin C} \frac{\rho_{\mathrm{vol}}^{\mathrm{pol}}(\mathbf{r}')}{|\mathbf{r} - \mathbf{r}'|}\mathrm{d}\mathbf{r}' \\ &= \left(1 - \frac{1}{\varepsilon}\right)\langle \Psi | \sum_{i=1}^{N} \frac{\theta(\mathbf{r}_i)}{|\mathbf{r} - \mathbf{r}_i|} | \Psi \rangle\end{aligned} \tag{3}$$

where Ψ is the solute wave function and the θ function is equal to one outside the cavity and zero inside. We employ the VMC approach to compute the integral above by sampling a set of M configurations $(\mathbf{r}_1^{(k)},...,\mathbf{r}_N^{(k)})$ from the square of the wave function $|\Psi|^2$. The electrostatic potential can then be written as due to a set of n_c volume polarization charges,

$$\phi_{\mathrm{vol}}^{\mathrm{pol}}(\mathbf{r}) \approx \sum_{l=1}^{n_c} \frac{q_l}{|\mathbf{r} - \mathbf{r}_l|} \tag{4}$$

where the $n_c \leq N \times M$ point charges have charge $q_l = (1 - 1/\varepsilon)/M$ and positions corresponding to the sampled one-electron coordinates outside the cavity, $\mathbf{r}_l = \mathbf{r}_i^{(k)}$ if $\theta(\mathbf{r}_i^{(k)}) = 1$.

The surface polarization charge density, σ, is linked to the total electric field as

$$\sigma(\mathbf{r}) = \frac{1 - \varepsilon}{4\pi\varepsilon}\mathbf{n}_+ \cdot \mathbf{E}_-(\mathbf{r}) \tag{5}$$

where $\mathbf{n}_+$ is a versor pointing outside the cavity and $\mathbf{E}_-(\mathbf{r})$ is the total electric field evaluated at the surface immediately inside the cavity, with $\mathbf{E}(\mathbf{r}) = \mathbf{E}_{\mathrm{solute}}(\mathbf{r}) + \mathbf{E}_{\mathrm{surf}}(\mathbf{r}) + \mathbf{E}_{\mathrm{vol}}(\mathbf{r})$. Thus, at the end of a VMC run in the solvent, the normal component of the averaged solute field and of the field produced by volume polarization is computed while, for the field related to the surface polarization charge density, we use the relation

$$\mathbf{n}_+ \cdot \mathbf{E}_{\mathrm{surf}-}(\mathbf{r}) = -2\pi\sigma(\mathbf{r}) + \int_{\Sigma} \frac{\mathbf{n}_+ \cdot (\mathbf{r} - \mathbf{r}_a)}{|\mathbf{r} - \mathbf{r}_a|^3}\sigma(\mathbf{r}_a)\mathrm{d}a \tag{6}$$

where the integral is defined over the cavity surface Σ.

The surface charge distribution is discretized dividing the surface in elements (tesserae) of area a and placing point charges at the center of each of them. In our implementation, the number of point charges per unit surface, p, is fixed, and it is the same for all the spheres of the cavity. The surface charge density at the point $\mathbf{r}_k$ is then approximated as

$$\sigma(\mathbf{r}_k) \approx \frac{q_k}{a} \tag{7}$$

dx.doi.org/10.1021/ct500723s | J. Chem. Theory Comput. 2014, 10, 5528−5537

where the positions of the point charges are determined by minimizing the mutual repulsion of equal charges on the surface of a sphere of a given fixed radius.[45] The Poisson equation establishes the relation between the surface charge polarization and the nuclear and the electronic density of the solute (which also determines the volume polarization charges) as

$$q_k = \sum_j G_{kj}(\Sigma, \varepsilon)\mathbf{n}_+ \cdot [\mathbf{E}_{\mathrm{vol}}(\mathbf{r}_j) + \mathbf{E}_{\mathrm{solute}}(\mathbf{r}_j)] \tag{8}$$

where G_{kj} depends only on the shape of the cavity and on the solvent dielectric constant.

This equation must be self-consistently solved with the molecular wave function of the solute, which is optimized in the presence of the PCM solvation through the minimization of the energy functional:

$$E[\Psi] = \langle \Psi | \mathcal{H}_{\mathrm{elec}} | \Psi \rangle + \sum_{\alpha<\beta} \frac{Z_\alpha Z_\beta}{|\mathbf{R}_\alpha - \mathbf{R}_\beta|} + \frac{1}{2}\int \rho_{\mathrm{solute}}(\mathbf{r})[V_\sigma(\mathbf{r}) + V_{\mathrm{vol}}(\mathbf{r})]\mathrm{d}\mathbf{r} \tag{9}$$

where $\mathcal{H}_{\mathrm{elec}}$ is the electronic Hamiltonian. The density of the solute is given by the sum of the charges of the nuclei Z_α at positions $\mathbf{R}_\alpha$ and the electronic contribution:

$$\rho_{\mathrm{solute}}(\mathbf{r}) = \sum_\alpha Z_\alpha \delta(\mathbf{r} - \mathbf{R}_\alpha) + \rho_e(\mathbf{r}) \tag{10}$$

and the potential due to the surface and volume charges is given by

$$V_\sigma(\mathbf{r}) + V_{\mathrm{vol}}(\mathbf{r}) = \sum_k^{\mathrm{surf,vol}} \frac{q_k}{|\mathbf{r} - \mathbf{r}_k|} \tag{11}$$

The solute−solvent interaction term in the energy functional given in eq 9 corresponds to the polarization contribution to the free energy of solvation, which we denote as $\Delta G^{(\mathrm{pol})}$ in the following. In order to prevent divergences of the Coulomb interaction at the coalescence points, we introduce a small cutoff distance and, when the electron and the point charge are closer than this distance, we set the interaction equal to the value it takes at the cutoff.

To describe the solute, we employ a many-body molecular wave function of the Jastrow−Slater form,

$$\Psi = \mathcal{J} \sum_{i=1}^{N_{\mathrm{CSF}}} c_i C_i \tag{12}$$

where c_i are the expansion coefficients of the CSFs, C_i, and $\mathcal{J}$ is the Jastrow correlation factor which has an explicit dependence on the interparticle distances. At a given geometry of the solute, the wave function is fully optimized by energy minimization within VMC in a state-specific or state-average fashion and brought to self-consistence with the surface and volume polarization charges through two cycles of generation of the solvent charges and optimization of the solute wave function for the targeted excited state.

2.2. Computation of the Forces in PCM. The inclusion of the PCM requires, however, some attention in the computation of the QMC forces by finite difference (as well as analytically) since the surface and volume polarization charges depend on the positions of the nuclear coordinates of the solute. When the atomic displacements are performed to compute the numerical forces, the spheres of the cavity centered on the atoms, and therefore, the point charges on the surface, must be rigidly moved with the atoms when the energy of the solute (eq 9) is evaluated at the displaced positions. Furthermore, the magnitude of the charges must be modified to account for the change of the electronic density distribution.[46]

We give here the details of our procedure and start by considering a small variation of an internal coordinate x_γ with respect to the starting configuration $\mathbf{x}$, where we have minimized the energy functional (eq 9) self-consistently with the solvent. The wave function of the solute is recentered and the atomic cavity spheres are rigidly moved with the nuclear centers. The contribution to the forces due to the solvent polarization is then computed as

$$\frac{\partial \Delta G^{(\mathrm{pol})}}{\partial x_\gamma} = \frac{[\Delta G^{(\mathrm{pol})}(\mathbf{x} + \delta x_\gamma) - \Delta G^{(\mathrm{pol})}(\mathbf{x} - \delta x_\gamma)]}{2\delta x_\gamma} \tag{13}$$

where $\Delta G^{(\mathrm{pol})}$ consists of two contributions, one from the volume charges and one from the surface charges as described above. The volume polarization charges do not change the value in the molecular deformation but must be repositioned according to the solute wave function recentering. To this end, we resort to the space-warp coordinate transformation of ref 47. Once this operation is complete, the volume contribution to the force is directly evaluated by means of the finite difference.

The surface polarization term is treated differently to avoid the self-consistent recalculation of the surface charges. To explain our procedure, it is convenient to rewrite $\Delta G^{(\mathrm{pol})}_{\mathrm{surf}}$ as the following:

$$\Delta G^{(\mathrm{pol})}_{\mathrm{surf}} = \frac{1}{2}\int \rho_{\mathrm{solute}}(\mathbf{r}) V_\sigma(\mathbf{r})\mathrm{d}\mathbf{r} = \frac{1}{2}\sum_k V_{\mathrm{solute}}(\mathbf{r}_k) q_k = \frac{1}{2}\sum_{kj} V_{\mathrm{solute}}(\mathbf{r}_k) G_{kj}\mathbf{n}_+ \cdot [\mathbf{E}_{\mathrm{vol}}(\mathbf{r}_j) + \mathbf{E}_{\mathrm{solute}}(\mathbf{r}_j)] \tag{14}$$

where we used eqs 8 and 9, and $V_{\mathrm{solute}}(\mathbf{r}_k)$ is the solute electrostatic potential at the center of surface element k. We can rewrite this equation in matrix form as

$$\Delta G^{(\mathrm{pol})}_{\mathrm{surf}} = \frac{1}{2}\mathbf{VGE} \tag{15}$$

where the row vector $\mathbf{V}$ represents the potential of the solute and the column vector $\mathbf{E}$ the electric field normal components. Consequently, eq 13 becomes

$$\frac{\partial \Delta G^{(\mathrm{pol})}_{\mathrm{surf}}}{\partial x_\gamma} = \frac{\left[\frac{1}{2}\mathbf{V}_+\mathbf{G}_+\mathbf{E}_+ - \frac{1}{2}\mathbf{V}_-\mathbf{G}_-\mathbf{E}_-\right]}{2\delta x_\gamma} \tag{16}$$

where the subscript ± indicates that the calculation is performed at $\mathbf{x} \pm \delta x_\gamma$. In the limit of $\delta x_\gamma \to 0$, we can neglect second and higher order terms in the variation of each quantity depending on $\boldsymbol{x}$, and write

$$\frac{\partial \Delta G^{(\mathrm{pol})}_{\mathrm{surf}}}{\partial x_\gamma} = [\mathbf{V}_+\mathbf{G}_+\mathbf{E}_0 + \mathbf{V}_0\mathbf{G}_0\mathbf{E}_+ - \mathbf{V}_-\mathbf{G}_-\mathbf{E}_0 - \mathbf{V}_0\mathbf{G}_0\mathbf{E}_-]/4\delta x_\gamma \tag{17}$$

where the subscript 0 labels quantities evaluated at the initial position $\mathbf{x}$. In order to avoid the recalculation of the electric

dx.doi.org/10.1021/ct500723s | J. Chem. Theory Comput. 2014, 10, 5528−5537

field at the displaced positions of surface charges, we introduce the following approximation,

$$\mathbf{V}_0\mathbf{G}_0\mathbf{E}_\pm \approx \mathbf{V}_\pm\mathbf{G}_\pm\mathbf{E}_0 \tag{18}$$

which is motivated by the bilinear form of the energy associated with the electrostatic field. This relation is exact in the case of a solute completely enclosed in a fixed cavity and for the nondiscretized treatment of the surface polarization distribution. With this approximation, the above derivative becomes

$$\frac{\partial \Delta G_{\mathrm{surf}}^{(\mathrm{pol})}}{\partial x_\gamma} \approx [2\mathbf{V}_+\mathbf{G}_+\mathbf{E}_0 - 2\mathbf{V}\_\mathbf{G}\_\mathbf{E}_0]/4\delta x_\gamma \tag{19}$$

We are aware that, through this simplification, we are neglecting small contributions of pure geometrical origin. We expect that such effects are generally negligible except for more complicated cavities than those considered in this work, that is, in case of very large solutes with cavity spheres non-centered on nuclei.

To assess the accuracy of our VMC/PCM scheme for the computation of the forces, we investigate the consistency between the energy profile and the computed forces for the LiF molecule, which is a simple system expected to strongly respond to the presence of a polar solvent such as water. We employ a single-determinant Jastrow−Slater wave function and plot the corresponding ground-state energy as a function of the bond length in the gas phase and in the PCM in Figure 1. For each geometry, the wave function is fully optimized in energy minimization and the surface and volume charges of the water environment are determined self-consistently. We then compare the force obtained as minus the derivative of the fit of the energy with the values of the numerical gradients computed with the scheme described above. Clearly, the forces computed at each geometry lie on the curve obtained by differentiating the fit of the energy and the consistency between energy and forces is equally good in the gas phase and in the presence of the PCM. This also demonstrates that the geometrical term we neglect in eq 19 gives a negligible contribution, smaller than the statistical error on the force. We expect that this approximation is similarly good for the molecules studied here since the shape of their cavities is also rather simple and does not present the complexity one can for instance encounter in the folding of a molecular chain.

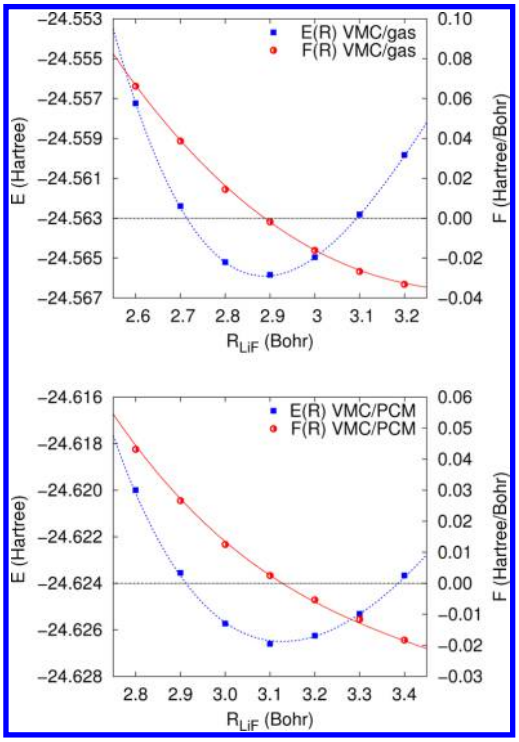

Figure 1. Energy (left scale) and force (right scale) of the LiF molecule as a function of the internuclear distance in the gas phase (above) and in PCM water solution (below). The dashed (blue) curve is a polynomial fit to the calculated energies and the solid (red) curve is minus the gradient of the fit. The forces (circles) are calculated as described in the text. The statistical errors are smaller than the symbol size.

3. COMPUTATIONAL DETAILS

We perform the TDDFT calculations with the Gaussian09 program[48] and employ the B3LYP,[49,50] PBE0,[51−53] M06,[54] M06-2X,[54] and CAM-B3LYP[55] exchange-correlation functionals. These functionals represent a subset of those considered in our previous gas-phase study[34] and have also been used in a recent investigation of TDDFT structures in solution.[12,13,18−20] We use the MOLCAS 7.2 suite of programs[56] for the CASPT2[57,58] calculations, and always employ the recommended zero-order Hamiltonian[27] with the IPEA shift set to 0.25 au.

The QMC calculations are carried out with the program package CHAMP.[59] We employ scalar-relativistic energy-consistent Hartree−Fock pseudopotentials[60,61] and obtain the starting determinantal component of the Jastrow−Slater wave function in complete-active-space self-consistent field (CASSCF) calculations performed with the program GAMESS-(US).[62] The CAS expansions are then expressed on the CASSCF natural orbitals and all configuration state functions (CSF) are retained in the QMC studies of acrolein, methylenecyclopropene, and acetone. For the excited state of the propenoic acid anion, the expansion is truncated imposing a threshold of 0.05 on the CSF coefficients and the union of the surviving CSF in the ground and excited states are then kept in the final wave functions. We employ a three-body Jastrow factor to account for electron−nuclear, electron−electron, and electron−electron−nucleus correlations and use different Jastrow factors to describe different atom types.[63] The difference between the VMC structures optimized with a two-body and a three-body Jastrow factor is rather small, between 0.003 and 0.006 Å in the gas phase and 0.003−0.009 Å in the PCM, and a good cancellation of errors is generally observed in the bond-length differences (see Supporting Information). In the following, we present the results obtained with the more sophisticated three-body Jastrow factor. The QMC wave functions are fully optimized within variational Monte Carlo using the linear method[33] and its extension to state-average calculations.[21]

We perform the CASPT2 and TDDFT calculations with the Dunning's correlation consistent cc-pVTZ basis set[64−67] and the QMC calculations with the basis sets specifically constructed for our pseudopotentials.[60] In particular, in QMC, we employ the cc-pVTZ' basis set, which consists of the cc-pVTZ for the heavy atoms and the cc-pVDZ basis set for hydrogen. For these molecules, this choice of basis sets represents a good compromise between accuracy and computational cost in the computation of the bond-length differences between PCM and the gas phase. With respect to the use of

dx.doi.org/10.1021/ct500723s | J. Chem. Theory Comput. 2014, 10, 5528−5537

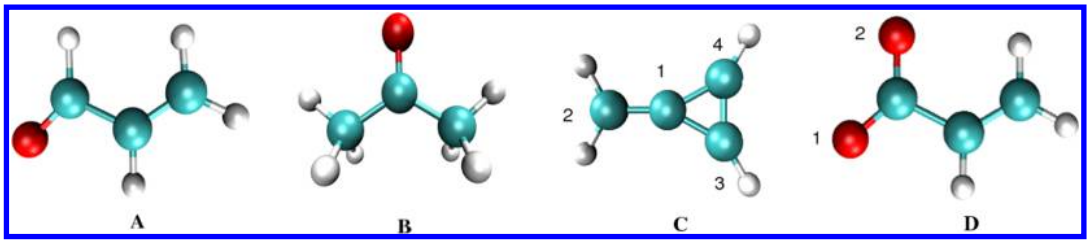

Figure 2. Molecules considered in this work: (A) *s*-trans acrolein, (B) acetone, (C) methylenecyclopropene (MCP), and (D) the propenoic acid anion (PAA).

augmentation, the largest basis-set error on this difference is observed for the very responsive $\pi \rightarrow \pi^*$ state of acrolein and amounts to 0.004 and 0.006 Å at the TDDFT and the CASPT2 level, respectively. Further details on the basis-set convergence are given in the Supporting Information.

For all PCM calculations, we construct the cavity using interlocking spheres centered on the nuclei, whose radii yield an electronic isodensity surface of 0.001 au. The radii of the spheres used for the different molecules are reported in the Supporting Information. In the VMC/PCM calculations, we include both surface and volume polarization charges[36] while the latter are not present in the TDDFT and CASPT2 calculations. In the TDDFT computations, we use the integral equation formalism variant of PCM (IEFPCM) while, in CASPT2, we use the standard PCM implemented in MOLCAS. In the CASPT2/PCM, the surface charges are computed self-consistently in the CASSCF step[41] and then simply included unchanged in the zero-order CASPT2 Hamiltonian. As starting geometry of the PCM excited-state optimizations, we use the corresponding optimal excited-state geometries obtained in the gas phase at the same level of theory.

As detailed in previous work by our group,[22,34] the VMC geometry optimization is performed in Z-matrix coordinates with numerical gradients of the energy with respect to the nuclear coordinates. The interatomic forces at a reference geometry are computed in a correlated sampling VMC calculation,[47] where a set of secondary geometries is generated through forward and backward displacements of 0.001 au in the bond lengths and 0.01 degrees in the bond and dihedral angles. To obtain finite-variance estimates of the gradients, we sample a distribution which is finite at the origin following ref 29. The VMC/PCM structural optimizations require generally about 5 iterations to converge to a final value of the interatomic gradients of about 0.001−0.003 Hartree/Bohr for the bond lengths and 0.0001 Hartree/degree for the bond angles. We then perform 5−8 additional steps after convergence to obtain the average estimates of the optimal internal coordinates.

4. RESULTS

The molecules considered in this work are the *s*-trans acrolein, acetone, methylenecyclopropene (MCP), and the propenoic acid anion (PAA), which are shown in Figure 2. The ground- and excited-state properties of these molecules have been extensively investigated in the gas phase with many different quantum chemical methods and are commonly employed to benchmark the quality of the predicted excited-state structures.[15,34,68−77] Relatively few studies have instead been performed on the effect of solvation on the ground- and excited-state equilibrium geometries of these molecules[15−17,19] and these studies suffered from the lack good reference data for comparison.

As in our gas-phase study,[34] we investigate the optimal structures of the $n \rightarrow \pi^*$ state of acrolein, acetone, and PAA, and of the $\pi \rightarrow \pi^*$ state of acrolein and MCP, imposing the symmetry constraints detailed in Table 1. For these states, we optimize the molecular geometries within VMC and CASPT2 and compare the relative performance of these correlated methods to the TDDFT structures obtained with several approximate exchange-correlation functionals. Here, we will focus on the effect of the solvation PCM environment on the equilibrium geometries, which is quantified in terms of bond-length differences with respect to the corresponding gas-phase structures.

Table 1. Symmetries Imposed in the Structural Optimization of the Low-Lying Excited States of the Molecules[a]

molecule	symmetry	state	excitation
s-trans acrolein	C_s	$1^1A''$	$n \rightarrow \pi^*$
		$2^1A'$	$\pi \rightarrow \pi^*$
acetone	C_{2v}	1^1A_2	$n \rightarrow \pi^*$
	C_s	$1^1A''$	$n \rightarrow \pi^*$
MCP	C_{2v}	1^1B_2	$\pi \rightarrow \pi^*$
PAA	C_s	$1^1A''$	$n \rightarrow \pi^*$

[a]The symmetry of the state and the nature of the excitation are also reported.

4.1. Acrolein. In the CASPT2 and VMC calculations of the $n \rightarrow \pi^*$ state of planar acrolein, we use a CAS(6,5) expansion given by four π orbitals on the conjugated carbon chain and one σ orbital describing a lone pair in the direction orthogonal to the CO group. In the $\pi \rightarrow \pi^*$ state, we employ a CAS(4,4) expansion over four π orbitals in VMC and a smaller CAS(2,2) in CASPT2. Both in the gas phase and in PCM, a CASSCF calculations with a CAS(4,4) expansion results in the bright $\pi \rightarrow \pi^*$ state being the third root in the A′ irreducible representation, which then becomes the second root when dynamical correlation is introduced with the perturbation correction or with the Jastrow factor in VMC. While the VMC optimization with a CAS(4,4) does not pose any problem, the CASPT2 calculations are affected by a strong mixing between the second and third eigenvectors at the multistate level, and therefore a perturbation wave function dramatically different from the zero-order reference. To better illustrate these difficulties, we report the spread of optimal geometries obtained with different active spaces at the single- and multistate CASPT2 level in the Supporting Information. Therefore, consistent with the choice made in the gas phase, we employ a different active space for the CASPT2 and VMC optimizations of the $\pi \rightarrow \pi^*$ structure, keeping in mind that the use of the small CAS(2,2) active space leads to a

straightforward CASPT2 optimization of the second state but may be variationally rather poor.

The optimal excited-state geometries of *s*-trans acrolein in the gas phase and solvation are shown in Figures 3 and 4, and

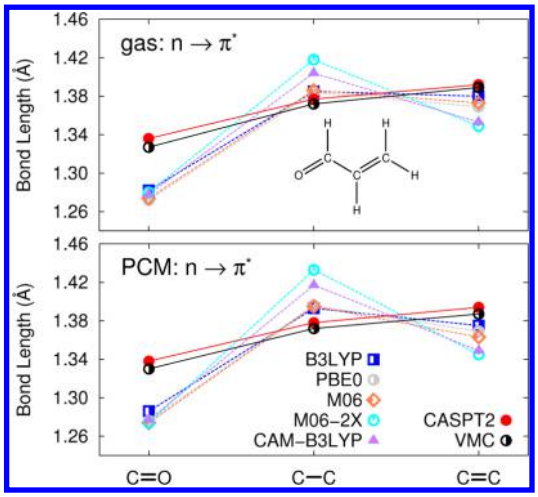

Figure 3. Bond lengths (Å) in the gas phase (top) and in water solution (bottom) of the $n \rightarrow \pi^*$ excited state of *s*-trans acrolein. The statistical error on the VMC values is about 0.001 Å.

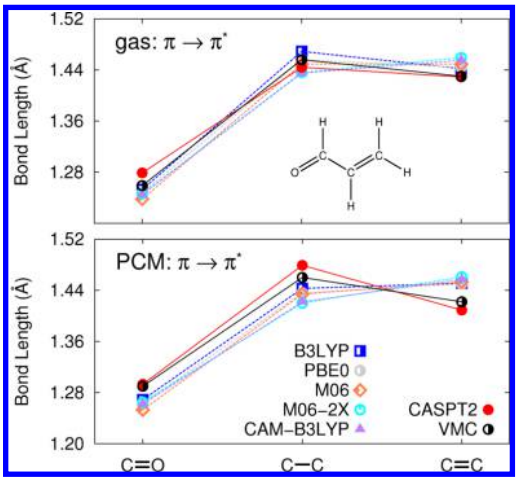

Figure 4. Bond lengths (Å) in the gas phase (top) and in water solution (bottom) of the $n \rightarrow \pi^*$ excited state of *s*-trans acrolein. The statistical error on the VMC values is smaller than 0.001 Å.

the bond-length differences between water and the gas phase are reported in Figure 5. In the $n \rightarrow \pi^*$ state, we find that VMC and CASPT2 agree in predicting that single and double bonds acquire a more similar length in the excited state and that this pattern is preserved in the PCM environment. The structural response of acrolein to solvation at the correlated level is in fact very small with changes in the bond lengths with respect to the gas phase well below 0.005 Å. All TDDFT functionals give instead double bonds in the excited state significantly shorter than the single one, and the difference is enhanced upon solvation: The single C–C bond lengthens by about 0.01–0.015 Å with respect to the gas phase, while the effect on the other bonds is much smaller (with the exception of the C═C bond optimized with the M06 functional which shortens by about 0.01 Å). These findings are consistent with a recent TDDFT study[19] where an even less polar solvent than water (acetonitrile) was considered.

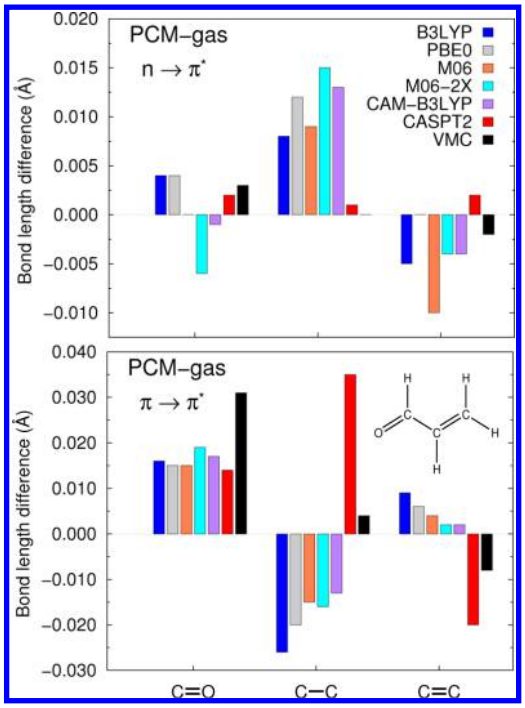

Figure 5. Bond-length differences (Å) between the geometries computed in water solution and in the gas phase for the $n \rightarrow \pi^*$ (top) and $\pi \rightarrow \pi^*$ (bottom) excited states of *s*-trans acrolein. The statistical error on the VMC bond-length differences is about 0.001 Å for the $n \rightarrow \pi^*$ and smaller than 0.001 Å for the $\pi \rightarrow \pi^*$ state. The CASPT2 geometry of the $\pi \rightarrow \pi^*$ state is obtained with a suboptimal CAS(2,2) active space (see text).

The geometry of the $\pi \rightarrow \pi^*$ state responds more strongly to the presence of water at the correlated level. This is expected since the dipole moment increases going from the ground to the $\pi \rightarrow \pi^*$ excited state, while it decreases in the $n \rightarrow \pi^*$ excited state.[42] The VMC and CASPT2 methods predict the same behavior upon solvation, namely, the elongation of the C═O and C—C bonds, and the shortening of the C═C bond. As discussed above, the absolute differences between the two correlated approaches must be attributed to the use of a suboptimal CAS(2,2) active space for CASPT2, and we will therefore use VMC as reference for the geometry optimization of this state. All TDDFT functionals yield an elongation of the carbonyl bond but display a change opposite to VMC in the carbon–carbon distances, that is, a shortening of the C—C bond by about 0.02 Å and a slight lengthening of the C═C bond.

Finally, in Figure 6, we compare our correlated results with the structural response of SAC-CI and CCSD in PCM water computed in refs 15 and 17, respectively. For the $n \rightarrow \pi^*$ state, CCSD slightly overestimates the geometrical response to the solvent and SAC-CI displays the same trend further amplifying the error with respect to CCSD. In the $\pi \rightarrow \pi^*$ state, while SAC-CI and CCSD yield the same pattern as VMC in the bond-length differences between PCM and gas-phase structures, both methods predict an excessive elongation of the C–C bond upon solvation by 0.04 and 0.03 Å, respectively.

4.2. Acetone. We optimize the $n \rightarrow \pi^*$ excited state of acetone in a planar C_{2v} structure corresponding to a saddle point of the potential energy surface and in the C_s minimum characterized by the pyramidalization of the central carbon atom out of the plane. In the CASPT2 and VMC computations,

dx.doi.org/10.1021/ct500723s | J. Chem. Theory Comput. 2014, 10, 5528–5537

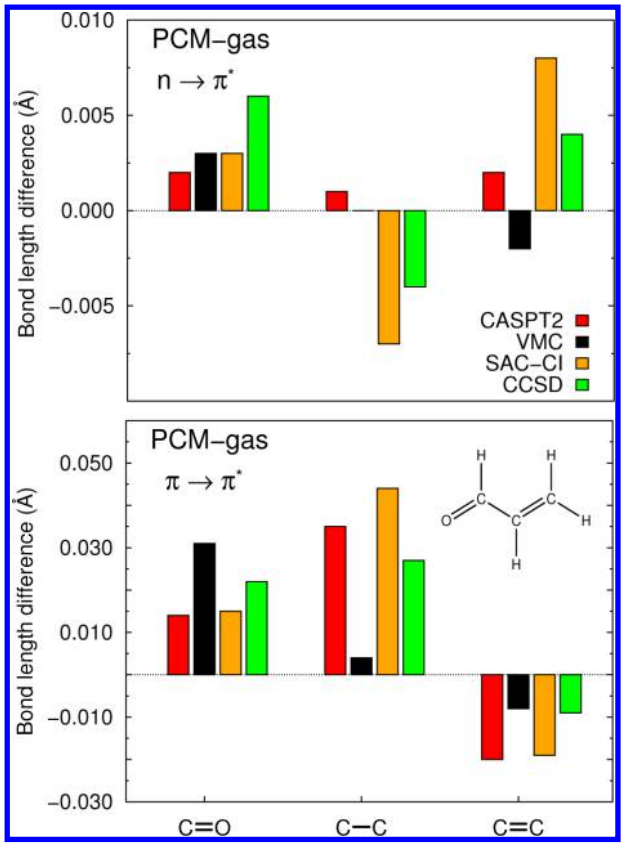

Figure 6. CASPT2 and VMC bond-length differences (Å) between the acrolein geometries computed in water solution and in the gas phase compared with SAC-CI[15] and CCSD[17] values from the literature. The CASPT2 geometry of the $\pi \rightarrow \pi^*$ state is obtained with a suboptimal CAS(2,2) active space (see text). The statistical error on the VMC bond-length differences is about 0.001 Å for the $n \rightarrow \pi^*$ and smaller than 0.001 Å for the $\pi \rightarrow \pi^*$ state.

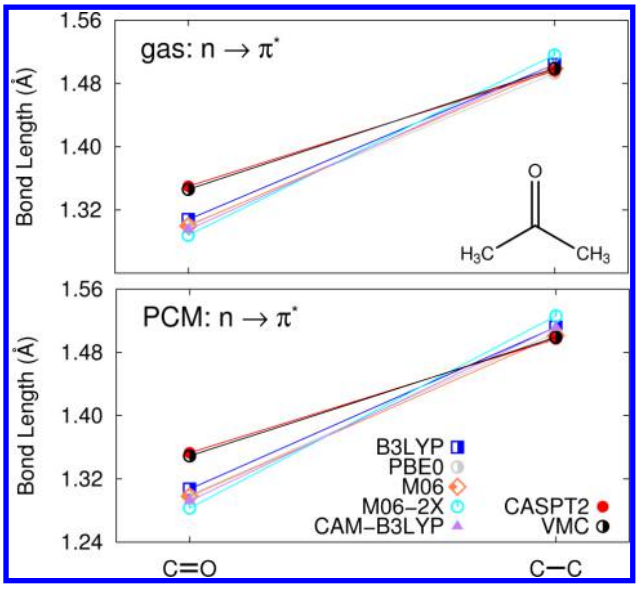

Figure 7. Bond lengths (Å) in the gas phase (top) and in water solution (bottom) of the $n \rightarrow \pi^*$ state of acetone. The statistical error on the VMC values is smaller than 0.001 Å.

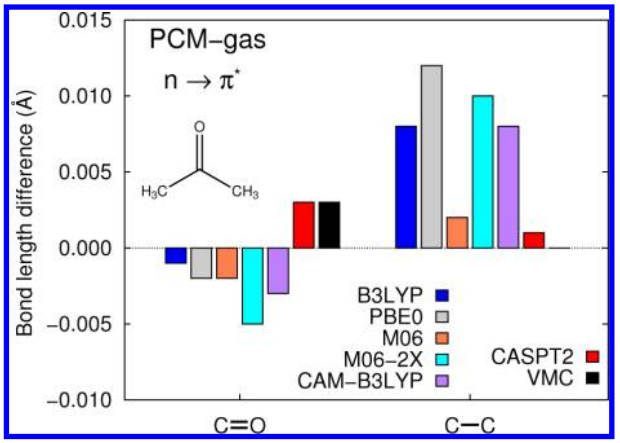

Figure 8. Bond length differences (Å) between the geometries computed in water solution and in the gas phase for the $n \rightarrow \pi^*$ state of acetone. The statistical error on the VMC bond-length differences is smaller than 0.001 Å.

the active space comprises four electrons in three orbitals, that is, the bonding and antibonding π orbitals on the CO bond, and the nonbonding lone pair on the oxygen. Here, we only discuss the C_s minimum structure and report all results for planar acetone in the Supporting Information since the response of both conformations to solvation is rather similar.

The excited-state geometries optimized in the gas phase and in water solution are shown in Figure 7 and the corresponding bond-length differences in Figure 8. All TDDFT functionals yield an optimal solvated structure with the carbonyl bond slightly shorter than in the gas phase and with the CC bonds longer by about 0.005−0.01 Å depending on the functional. As in the case of the $n \rightarrow \pi^*$ state of acrolein, CASPT2 and VMC display a different response to solvation than TDDFT yielding no appreciable changes in the optimized geometries with respect to the gas phase: The VMC bond-length difference on the CC bond is zero within statistical error and on the CO bond below 0.005 Å, consistently with CASPT2.

4.3. Methylenecyclopropene. In planar MCP, the dipole moment in the $\pi \rightarrow \pi^*$ excited state lies along the $C_1{=}C_2$ bond and has similar magnitude but opposite direction than in the ground state. More precisely, the dipole moment points toward the exocyclic bond in the ground state and toward the ring in the excited state, reflecting a flux of charge in the same direction upon excitation. This remarkable variation in the distribution of the electronic density leads to the simultaneous shortening of the $C_1{=}C_2$ bond and the lengthening of the $C_1{-}C_3$ and $C_3{=}C_4$ bonds in the excited state.[34,42] The $\pi \rightarrow \pi^*$ excited state of MCP in water is optimized maintaining planarity and using at the correlated level a CAS(4,4) reference wave function, which includes the two bonding and two antibonding π orbitals.

As shown in Figures 9 and 10, the effect of introducing a solvation environment is rather small and of the order of mÅ both in VMC and in CASPT2. All TDDFT functionals predict instead that the change in the bond-length pattern observed upon excitation in the gas phase is emphasized in water: The $C_1{=}C_2$ bond becomes consistently shorter by about 0.015 Å, while the $C_1{-}C_3$ and $C_3{=}C_4$ bonds are slightly elongated. Finally, we compare the CASPT2 and VMC bond-length differences with the SAC−CI values from ref 15 in Figure 11. Again, we find that SAC−CI yields significant deviations on the excited-state structures not only in the gas phase[34] but also in response to solvation.

dx.doi.org/10.1021/ct500723s | J. Chem. Theory Comput. 2014, 10, 5528−5537

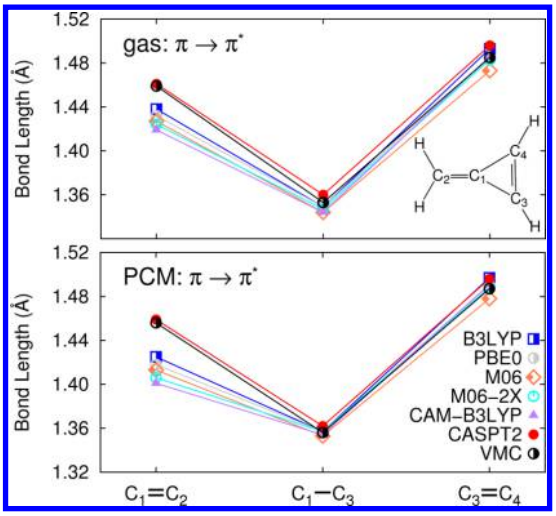

Figure 9. Bond lengths (Å) in the gas phase (top) and in water solution (bottom) of the $\pi \rightarrow \pi^*$ state of MCP. The statistical error on the VMC values is smaller than 0.001 Å.

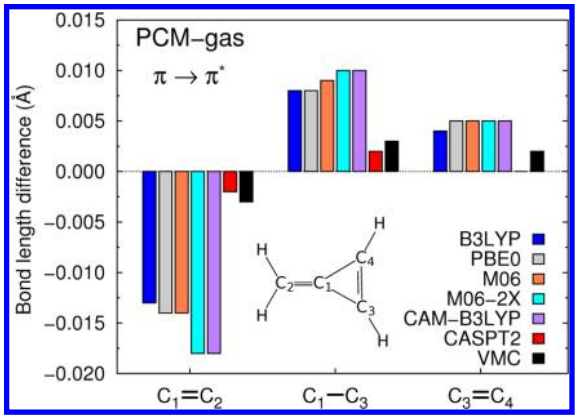

Figure 10. Bond-length differences (Å) between the geometries computed with in water solution and in the gas phase for the $\pi \rightarrow \pi^*$ state of MCP. The statistical error on the VMC bond-length differences is smaller than 0.001 Å.

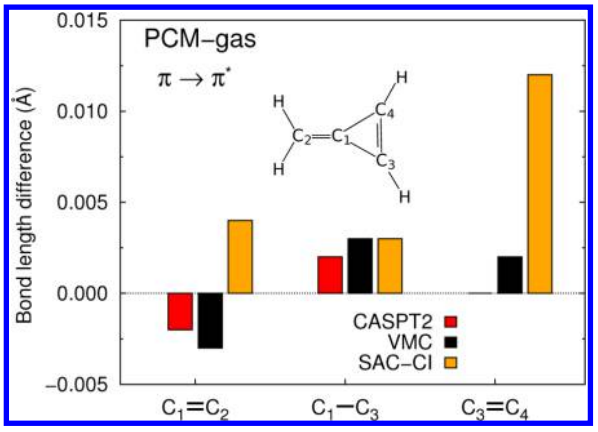

Figure 11. CASPT2 and VMC bond-length differences (Å) between the geometries computed in water solution and in the gas phase for the $\pi \rightarrow \pi^*$ state of MCP, compared with the SAC−CI values from ref 15. The statistical error on the VMC bond-length differences is smaller than 0.001 Å.

4.4. Propenoic Acid Anion. The last molecule considered in this work is the propenoic acid anion in its $n \rightarrow \pi^*$ excited state. For the CASPT2 and VMC optimizations, we use a CAS(10,7) expansion, which includes five π orbitals on the conjugated chain and two σ orbitals on the oxygen atoms to describe the lone pairs. We employed this same active space in the gas-phase optimizations of our previous study,[34] where we showed how the choice of a smaller active space with only one of the two lone pairs leads to excited-state geometries with a differential elongation of the $C-O_1$ and $C-O_2$ bonds, depending on which lone pair is added to the active space.

The excited-state geometries of PAA in water and in the gas phase, and their difference are shown in Figures 12 and 13. The

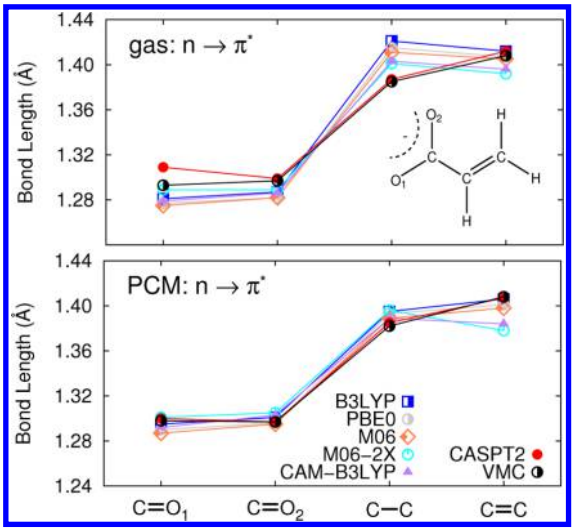

Figure 12. Bond lengths (Å) in the gas phase (top) and in water solution (bottom) of the $n \rightarrow \pi^*$ state of PAA. The statistical error on the VMC values is smaller than 0.001 Å.

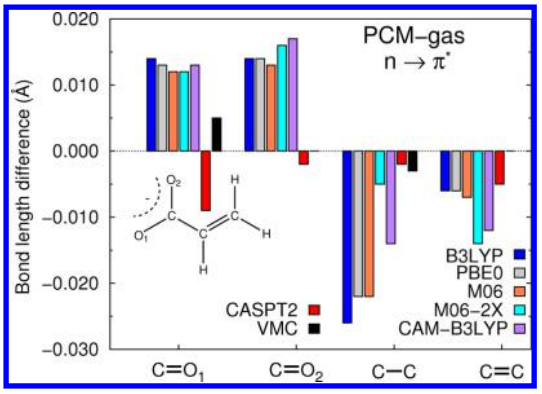

Figure 13. Bond-length differences (Å) between the geometries computed in water solution and in the gas for the $n \rightarrow \pi^*$ state of PAA. The statistical error on the VMC bond-length differences is smaller than 0.001 Å.

effect of PCM on the CASPT2 geometries is to slightly shorten all bonds with respect to the gas phase, while the VMC response to the presence of the solvent is almost zero. As in the case of the other molecules, the response of TDDFT is stronger with the CC bonds shortening by 0.01−0.02 and the CO bonds lengthening by about 0.01−0.02 Å. These results are consistent with what reported in a recent TDDFT structural study in a solvated PCM environment.[19]

dx.doi.org/10.1021/ct500723s | J. Chem. Theory Comput. 2014, 10, 5528−5537

5. CONCLUSIONS

This work combines for the first time the PCM model of solvation with QMC techniques to perform geometry optimizations in the ground and excited states. We consider here a set of chromophores in water representative of $n \rightarrow \pi^*$ and $\pi \rightarrow \pi^*$ excitations and compute the optimal excited-state geometries with the QMC method in its simplest VMC variant, coupled to the PCM description of the solvent. Importantly, in our implementation of the PCM model, the reaction field includes both volume and surface polarization charges and is determined self-consistently with the molecular wave function during the QMC optimization of the solute geometry. These features must be contrasted to common implementations of the PCM model where the volume charges are not introduced or the response of the reaction field is not taken into account at the same level of theory as in the CASPT2 calculations. The consistency between the energy profile and the forces computed with our VMC/PCM approach is demonstrated for the test case of LiF, a simple molecule whose structure strongly responds to a polar solvent such as water.

To establish the robustness of our scheme as well as offer reliable reference data for TDDFT in solution, we compare the excited-state QMC geometries of the selected chromophores in water to the structures we optimized with CASPT2 and a variety of TDDFT functionals. The geometrical response to the solvent estimated in QMC is found to be in very good agreement with the predictions of the CASPT2 method, with the only exception of the $\pi \rightarrow \pi^*$ state of acrolein where one must use the computational expedient of a suboptimal active space at the perturbation level while no such compromise is needed in the QMC optimization of this excited state.

As regards TDDFT, we find that the functionals investigated here generally overestimate the geometrical variations in the excited states due to the presence of the solvent, further increasing the discrepancy with the correlated approaches already observed in the gas phase. The $\pi \rightarrow \pi^*$ excited state of acrolein is the only state which sees a non-negligible structural response to solvation also at the correlated level with QMC bond-length differences with respect to the gas phase as large as 0.03 Å. However, while VMC and CASPT2 predict the elongation of the C—C and the shortening of the C═C bond in solution, all TDDFT functionals yield the opposite behavior.

In conclusion, we have demonstrated that QMC in its simplest VMC flavor is an accurate method for structural optimization in the presence of PCM solvation. Thanks to its favorable computational scaling as compared to other correlated approaches, our QMC scheme self-consistently coupled to the reaction field via surface and volume charges is therefore a robust and promising approach to investigate the structural relaxation and fluorescence in solution of also larger molecules with higher accuracy than present TDDFT functionals.

■ ASSOCIATED CONTENT

Supporting Information

Geometries optimized in PCM for all molecules and states. Study of the basis-set convergence and analysis of the choice of cavity parameters. This material is available free of charge via the Internet at http://pubs.acs.org.

■ AUTHOR INFORMATION

Corresponding Authors

*E-mail: floris@dcci.unipi.it.
*E-mail: claudio.amovilli@unipi.it.
*E-mail: c.filippi@utwente.nl.

Notes

The authors declare no competing financial interest.

■ ACKNOWLEDGMENTS

We thank B. Mennucci for useful discussions. R.G. is supported by an ECHO grant (712.012.005) of The Netherlands Organisation for Scientific Research (NWO). We acknowledge support from NWO for the use of the SARA supercomputer facilities, from the COST Action CODECS and from MIUR under project PRIN 2009.

■ REFERENCES

(1) Tomasi, J.; Mennucci, B.; Cammi, R. *Chem. Rev.* **2005**, *105*, 2999−3094.
(2) Lin, H.; Truhlar, D. *Theor. Chem. Acc.* **2007**, *117*, 185−199.
(3) Senn, H. M.; Thiel, W. *Angew. Chem., Int. Ed.* **2009**, *48*, 1198−1229.
(4) Seabra, G.; Swails, J.; Roitberg, A. In *Multi-Scale Quantum Models for Biocatalysis*; Springer: New York, 2009; Vol. 7; pp 3−20.
(5) Mennucci, B. *Phys. Chem. Chem. Phys.* **2013**, *15*, 6583−6594.
(6) Tomasi, J.; Persico, M. *Chem. Rev.* **1994**, *94*, 2027−2094.
(7) Barone, V.; Cossi, M. *J. Phys. Chem. A* **1998**, *102*, 1995−2001.
(8) Chipman, D. M. *J. Chem. Phys.* **2009**, *131*, 014104.
(9) Casida, M. *J. Mol. Struct.: THEOCHEM* **2009**, *914*, 3−18.
(10) Casida, M.; Huix-Rotllant, M. E. *Annu. Rev. Phys. Chem.* **2012**, *63*, 287−323.
(11) Marques, M.; Maitra, T. N.; Nogueira, F. M. S.; Gross, E. K. U.; Rubio, A. *Fundamentals of Time-Dependent Density Functional Theory*; Springer: Heidelberg, 2012; pp 53−99.
(12) Scalmani, G.; Frisch, J. M.; Mennucci, B.; Tomasi, J.; Cammi, R.; Barone, V. *J. Chem. Phys.* **2006**, *124*, 094107.
(13) Jacquemin, D.; Perpète, E. A.; Assfeld, X.; Scalmani, G.; Frisch, M. J.; Adamo, C. *Chem. Phys. Lett.* **2007**, *438*, 208−212.
(14) Clemens, O.; Basters, M.; Wild, M.; Wilbrand, S.; Reichert, C.; Bauer, M.; Springborg, M.; Jung, G. *J. Mol. Struct.: THEOCHEM* **2008**, *866*, 15−20.
(15) Cammi, R.; Fukuda, R.; Ehara, M.; Nakatsuji, H. *J. Chem. Phys.* **2010**, *133*, 024104.
(16) Caricato, M. *J. Chem. Theory Comput.* **2012**, *8*, 4494−4502.
(17) Caricato, M. *J. Chem. Theory Comput.* **2012**, *8*, 5081−5091.
(18) Jacquemin, D.; Planchat, A.; Adamo, C.; Mennucci, B. *J. Chem. Theory Comput.* **2012**, *8*, 2359−2372.
(19) Guido, C. A.; Knecht, S.; Kongsted, J.; Mennucci, B. *J. Chem. Theory Comput.* **2013**, *9*, 2209−2220.
(20) Chibani, S.; Laurent, A. D.; Blondel, A.; Mennucci, B.; Jacquemin, D. *J. Chem. Theory Comput.* **2014**, *10*, 1848−1851.
(21) Filippi, C.; Zaccheddu, M.; Buda, F. *J. Chem. Theory Comput.* **2009**, *5*, 2074−2087.
(22) Valsson, O.; Filippi, C. *J. Chem. theory Comput.* **2010**, *6*, 1275−1292.
(23) Send, R.; Valsson, O.; Filippi, C. *J. Chem. Theory Comput.* **2011**, *7*, 444−455.
(24) Filippi, C.; Buda, F.; Guidoni, L.; Sinicropi, A. *J. Chem. Theory Comput.* **2012**, *8*, 112−124.
(25) Valsson, O.; Angeli, C.; Filippi, C. *Phys. Chem. Chem. Phys.* **2012**, *14*, 11015−11020.
(26) Valsson, O.; Campomanes, P.; Tavernelli, I.; Rothlisberger, U.; Filippi, C. *J. Chem. Theory Comput.* **2013**, *9*, 2441−2454.
(27) Ghigo, G.; Roos, B. O.; Malmqvist, P.-Å. *Chem. Phys. Lett.* **2004**, *396*, 142−149.
(28) Angeli, C.; Cimiraglia, R.; Evengelisti, S.; Leininger, T.; Malrieu, J.-P. *J. Chem. Phys.* **2001**, *114*, 10252−10264.

(29) Attaccalite, C.; Sorella, S. *Phys. Rev. Lett.* **2008**, *100*, 114501.
(30) Sorella, S.; Capriotti, L. *J. Chem. Phys.* **2010**, *133*, 234111.
(31) Barborini, M.; Guidoni, L. *J. Chem. Phys.* **2012**, *137*, 224309.
(32) Saccani, S.; Filippi, C.; Moroni, S. *J. Chem. Phys.* **2013**, *138*, 084109.
(33) Umrigar, C. J.; Toulouse, J.; Filippi, C.; Sorella, S.; Hennig, R. G. *Phys. Rev. Lett.* **2007**, *98*, 110201.
(34) Guareschi, R.; Filippi, C. *J. Chem. Theory Comput.* **2013**, *9*, 5513−5525.
(35) Amovilli, C.; Filippi, C.; Floris, F. M. *J. Phys. Chem. B* **2006**, *110*, 26225−26231.
(36) Amovilli, C.; Filippi, C.; Floris, F. M. *J. Chem. Phys.* **2008**, *129*, 244106.
(37) Floris, F. M.; Filippi, C.; Amovilli, C. *J. Chem. Phys.* **2012**, *137*, 075102.
(38) Floris, F. M.; Filippi, C.; Amovilli, C. *J. Chem. Phys.* **2014**, *140*, 034109.
(39) Cammi, R.; Mennucci, B. *J. Chem. Phys.* **1999**, *110*, 9877−9886.
(40) Cossi, M.; Barone, V. *J. Chem. Phys.* **2001**, *115*, 4708−4717.
(41) Cossi, M.; Barone, V.; Rega, N.; Scalmani, G.; Barone, V. *J. Chem. Phys.* **2001**, *114*, 5691−5701.
(42) Caricato, M.; Mennucci, B.; Tomasi, J.; Ingrosso, F.; Cammi, R.; Corni, S.; Scalmani, G. *J. Chem. Phys.* **2006**, *124*, 124520.
(43) Jacquemin, D.; Planchat, A.; Adamo, C.; Mennucci, B. *J. Chem. Theory Comput.* **2012**, *8*, 2359−2372.
(44) Jacquemin, D.; Mennucci, B.; Adamo, C. *Phys. Chem. Chem. Phys.* **2011**, *13*, 16987−16998.
(45) Amovilli, C.; March, N. H. *Chem. Phys. Lett.* **2001**, *347*, 459−464.
(46) Cammi, R.; Tomasi, J. *J. Chem. Phys.* **1994**, *101*, 3888−3897.
(47) Filippi, C.; Umrigar, C. J. *Phys. Rev. B* **2000**, *61*, R16291−R16294.
(48) Frisch, M. J.; Trucks, G. W.; Schlegel, H. B.; Scuseria, G. E.; Robb, M. A.; Cheeseman, J. R.; Scalmani, G.; Barone, V.; Mennucci, B.; Petersson, G. A.; Nakatsuji, H.; Caricato, M.; Li, X.; Hratchian, H. P.; Izmaylov, A. F.; Bloino, J.; Zheng, G.; Sonnenberg, J. L.; Hada, M.; Ehara, M.; Toyota, K.; Fukuda, R.; Hasegawa, J.; Ishida, M.; Nakajima, T.; Honda, Y.; Kitao, O.; Nakai, H.; Vreven, T.; Montgomery, J. A., Jr.; Peralta, J. E.; Ogliaro, F.; Bearpark, M.; Heyd, J. J.; Brothers, E.; Kudin, K. N.; Staroverov, V. N.; Kobayashi, R.; Normand, J.; Raghavachari, K.; Rendell, A.; Burant, J. C.; Iyengar, S. S.; Tomasi, J.; Cossi, M.; Rega, N.; Millam, J. M.; Klene, M.; Knox, J. E.; Cross, J. B.; Bakken, V.; Adamo, C.; Jaramillo, J.; Gomperts, R.; Stratmann, R. E.; Yazyev, O.; Austin, A. J.; Cammi, R.; Pomelli, C.; Ochterski, J. W.; Martin, R. L.; Morokuma, K.; Zakrzewski, V. G.; Voth, G. A.; Salvador, P.; Dannenberg, J. J.; Dapprich, S.; Daniels, A. D.; Farkas, Ö.; Foresman, J. B.; Ortiz, J. V.; Cioslowski, J.; Fox, D. J. *Gaussian09*, Revision A.02; Gaussian Inc.: Wallingford, CT, 2009.
(49) Becke, A. D. *J. Chem. Phys.* **1993**, *98*, 5648−5652.
(50) Stephens, P. J.; Devlin, F. J.; Chabalowski, C. F.; Frisch, M. J. *J. Phys. Chem.* **1994**, *98*, 11623−11627.
(51) Perdew, J. P.; Burke, K.; Ernzerhof, M. *J. Chem. Phys.* **1996**, *105*, 9982−9985.
(52) Adamo, C.; Barone, V. *J. Chem. Phys.* **1999**, *110*, 6158−6170.
(53) Ernzerhof, M.; Scuseria, G. E. *J. Chem. Phys.* **1999**, *110*, 5029−5036.
(54) Zhao, Y.; Truhlar, D. *Theor. Chem. Acc.* **2008**, *120*, 215−241.
(55) Yanai, T.; Tew, D. P.; Handy, N. C. *Chem. Phys. Lett.* **2004**, *393*, 51−57.
(56) Karlström, G.; Lindh, R.; Malmqvist, P.-Å.; Roos, B. O.; Ryde, U.; Veryazov, V.; Widmark, P.-O.; Cossi, M.; Schimmelpfennig, B.; Neogrady, P.; Seijo, L. *Comput. Mater. Sci.* **2003**, *28*, 222−239.
(57) Andersson, K.; Malmqvist, P.-A.; Roos, B. O.; Sadlej, A. J.; Wolinski, K. *J. Phys. Chem.* **1990**, *94*, 5483−5488.
(58) Andersson, K.; Malmqvist, P.-A.; Roos, B. O. *J. Chem. Phys.* **1992**, *96*, 1218−1226.
(59) CHAMP is a quantum Monte Carlo program package written by Umrigar, C. J.; Filippi, C. and collaborators.
(60) Burkatzki, M.; Filippi, C.; Dolg, M. *J. Chem. Phys.* **2007**, *126*, 234105.
(61) For the hydrogen atom, we use a more accurate BFD pseudopotential and basis set. Dolg, M.; Filippi, C., private communication.
(62) Schmidt, M. W.; Baldridge, K. K.; Boatz, J. A.; Elbert, S. T.; Gordon, M. S.; Jensen, J. H.; Koseki, S.; Matsunaga, N.; Nguyen, K. A.; Su, S.; Windus, T. L.; Dupuis, M.; A. M, J., Jr. *J. Comput. Chem.* **1993**, *14*, 1347−1363.
(63) Filippi, C.; Umrigar, C. J. *J. Chem. Phys.* **1996**, *105*, 213−226 As Jastrow correlation factor, we use the exponential of the sum of three fifth-order polynomials of the electron−nuclear (e−n), the electron−-electron (e−e). The Jastrow factor is adapted to deal with pseudo-atoms, and the scaling factor k is set to 0.6 au. The 2-body Jastrow factor includes five parameters in the e−e terms and four parameters for each atom type in the e−n terms..
(64) Dunning, T. H., Jr. *J. Chem. Phys.* **1989**, *90*, 1007−1023.
(65) Peterson, K. A.; Woon, D. E.; Dunning, T. H., Jr. *J. Chem. Phys.* **1994**, *100*, 7410−7415.
(66) Wilson, A.; van Mourik, T.; Dunning, T. H., Jr. *J. Mol. Struct.: THEOCHEM* **1997**, *388*, 339−349.
(67) Weigend, F. *Phys. Chem. Chem. Phys.* **2006**, *8*, 1057−1065.
(68) Reguero, M.; Olivucci, M.; Bernardi, F.; Robb, M. A. *J. Am. Chem. Soc.* **1994**, *116*, 2103−2114.
(69) Gwaltney, S. R.; Bartlett, R. J. *J. Chem. Phys.* **1999**, *110*, 62−71.
(70) Aquilante, F.; Barone, V.; Roos, B. *J. Chem. Phys.* **2003**, *119*, 12323−12334.
(71) Page, S. C.; Olivucci, M. *J. Comput. Chem.* **2003**, *24*, 298−309.
(72) Angeli, C.; Borini, S.; Ferrighi, L.; Cimiraglia, R. *J. Chem. Phys.* **2005**, *122*, 114304.
(73) Angeli, C.; Borini, S.; Ferrighi, L.; Cimiraglia, R. *J. Mol. Struct.: THEOCHEM* **2005**, *718*, 55−69.
(74) Saha, B.; Ehara, M.; Nakatsuji, H. *J. Chem. Phys.* **2006**, *125*, 014316.
(75) Losa, A. M.; Galván, I. F.; Aguilar, M. A.; Martín, M. E. *J. Phys. Chem. B* **2007**, *111*, 9864−9870.
(76) Guido, C. A.; Jacquemin, D.; Adamo, C.; Mennucci, B. *J. Phys. Chem. A* **2010**, *114*, 13402−13410.
(77) Gadaczeck, I.; Krause, K.; Hintze, K. J.; Bredow, T. *J. Chem. Theory Comput.* **2012**, *8*, 986−996.